Complete temporal mode characterization of non-Gaussian states by a dual homodyne measurement

Kan Takase,[1,*] Masanori Okada,[1] Takahiro Serikawa,[1] Shuntaro Takeda,[1,2] Jun-ichi Yoshikawa,[1] and Akira Furusawa[1,†]

[1]*Department of Applied Physics, School of Engineering, The University of Tokyo, 7-3-1 Hongo, Bunkyo-ku, Tokyo 113-8656, Japan*
[2]*JST, PRESTO, 4-1-8 Honcho, Kawaguchi, Saitama 332-0012, Japan*

Optical quantum states defined in temporal modes, especially non-Gaussian states, such as photon-number states, play an important role in quantum computing schemes. In general, the temporal mode structures of these states are characterized by one or more complex functions called temporal mode functions (TMFs). Although we can calculate the TMF theoretically in some cases, experimental estimation of a TMF is more advantageous to utilize the states with high purity. In this paper, we propose a method to estimate complex TMFs. This method can be applied not only to arbitrary single temporal mode non-Gaussian states, but also to two temporal mode states containing two photons. This method is implemented by continuous-wave dual homodyne measurement and does not need prior information of the target states nor state reconstruction procedure. We demonstrate this method by analyzing several experimentally created non-Gaussian states.

I. INTRODUCTION

Quantum states of light are a promising resource of quantum computation [1–3] and quantum communication [4,5]. They are characterized by optical modes, such as polarization, spatial, and temporal modes. Among these modes, temporal modes have a lot of flexibility thus are useful for many applications. One prominent example is temporal mode multiplexing of quantum states to realize large-scale fault-tolerant quantum computation [3,6–11]. In this scheme, grasping temporal mode structures of quantum states is essential for basic operations, such as interference and measurement. Therefore, a methodology to characterize the states' temporal mode is in great demand.

A temporal mode f is characterized by a complex function $f(t)$, called the temporal mode function (TMF). For example, single-photon states in a temporal mode f are given by $|1_f\rangle \equiv \hat{a}_f^\dagger |\tilde{0}\rangle$, where $|\tilde{0}\rangle$ is a multimode vacuum state and $\hat{a}_f^\dagger \equiv \int dt\, f(t) \hat{a}^\dagger(t)$ is a creation operator of temporal mode f. Such non-Gaussian states, which can be used as ancillary states or a quantum information carrier in quantum computation, are the main interest of temporal mode analysis. Although we can calculate the TMFs theoretically in some state creation schemes [12], imperfection of experiment varies their actual forms. This mismatch leads to extra photon loss in useful applications. Therefore, experimental estimation of the TMFs of optical quantum states is essential to utilize the states with high purity.

So far, single temporal mode states, the states described by one temporal mode, have been actively analyzed experimentally. Especially, homodyne and heterodyne measurements are powerful tools both in continuous-wave (cw) and in pulse regimes. In Refs. [13,14], the TMFs are estimated by shaping the temporal modes of pulsed local oscillator (LO) beams for homodyne measurement. On the other hand, in the cw regime, temporal modes of LO beams are fixed, and the TMFs can be estimated by posteriorly processing the measurement results. Actually, the TMFs of single-photon states and Schrödinger's cat states are estimated [15–17] by applying principal component analysis (PCA) [18], which decomposes correlated variables into uncorrelated variables, to cw homodyne signals. This method does not require prior information of the target states and can access the TMFs without a state reconstruction algorithm. We can apply this method to arbitrary single temporal mode non-Gaussian states. However, their TMFs are limited to real functions because the PCA gives us only real functions. Reference [19] estimates complex TMFs of single-photon states by constructing what they call the temporal density matrix via cw heterodyne tomography. In the case of general non-Gaussian states, however, we need to consider a larger size density matrix having higher-photon number components, and estimation of the TMFs is not trivial. On top of that, we need several LO beams having different frequencies for the construction of a temporal density matrix.

In this paper, we propose a method that we call the *complex-number PCA (CPCA)*; estimation of complex TMFs by applying the PCA to complex variables given by cw dual homodyne measurement. Figure 1 is a conceptual diagram of our method. The CPCA can deal with arbitrary single temporal mode non-Gaussian states characterized by complex TMFs. On top of that, it can be applied to dual temporal mode states containing two photons $\hat{a}_{f_1}^\dagger \hat{a}_{f_2}^\dagger |\tilde{0}\rangle$ to estimate the complex TMFs $f_1(t)$, $f_2(t)$. These states are the simplest example of multitemporal mode states, which play an important role in useful applications [20–22]. Our method possibly opens a way to the TMF estimation of general multitemporal mode states. Like the previous PCA method, the CPCA needs no prior information, state reconstruction procedure, nor LO beams having different frequencies. The simplicity and capability of our method to characterize a wide range of quantum states

*takase@alice.t.u-tokyo.ac.jp
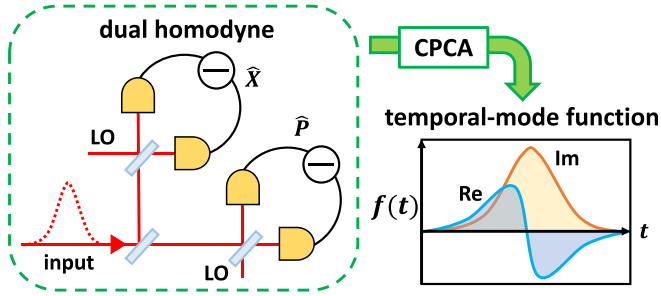†akiraf@ap.t.u-tokyo.ac.jp

FIG. 1. Conceptual diagram. The input state is a non-Gaussian state in unknown temporal modes. We estimate the temporal mode structure by measuring conjugate quadratures $\hat{X}, \hat{P}$ by dual homodyne measurement and processing the data by the CPCA.

would lead to useful applications not only in state creation experiments, but also in quantum communication and quantum computation schemes [1–5]. We experimentally demonstrate this method using several non-Gaussian states characterized by complex TMFs.

This paper is organized as follows. In Sec. II A, we define temporal modes of light and optical single and multitemporal mode quantum states. In Sec. II B, we review the previous estimation of real TMFs by the PCA. In Sec. II C, we discuss applying the PCA to cw dual homodyne measurement signals. In Sec. II D, we discuss how to analyze two-photon states $\hat{a}_{f_1}^\dagger \hat{a}_{f_2}^\dagger |\tilde{0}\rangle$. In Sec. II E, we discuss how photon loss affects our analysis. In Sec. II F, we summarize the application range of the CPCA. In Sec. III A, we review a creation method of non-Gaussian states. In Sec. III B, we explain the experimental setup. In Sec. III C, we show the experimentally estimated TMFs of several non-Gaussian states.

II. THEORY

A. Definition of temporal modes

We introduce optical TMFs and basic operators. A temporal mode f is characterized by time spectrum $f(t)$ called a TMF in which quantum states can be defined. The TMFs are complex functions in general. We define the instantaneous annihilation and creation operators $\hat{a}(t)$ and $\hat{a}^\dagger(t)$ which satisfy the commutation relation $[\hat{a}(t), \hat{a}^\dagger(t')] = \delta(t - t')$ where $\delta(t)$ is the Dirac-δ function. Then, photon annihilation and creation in a temporal mode f are described by operators given by

$$\hat{a}_f \equiv \int dt\, f^*(t)\hat{a}(t), \qquad \hat{a}_f^\dagger \equiv \int dt\, f(t)\hat{a}^\dagger(t). \quad (1)$$

Suppose the complex function $f(t)$ satisfies $\int dt |f(t)|^2 = 1$ so that these operators satisfy $[\hat{a}_f, \hat{a}_f^\dagger] = 1$. In general,

$$\begin{aligned}
\left[\hat{a}_{f_j}, \hat{a}_{f_k}^\dagger\right] &= \int dt \int dt'\, f_j^*(t) f_k(t') [\hat{a}(t), \hat{a}^\dagger(t')] \\
&= \int dt\, f_j^*(t) f_k(t) \\
&\equiv \langle f_j, f_k \rangle.
\end{aligned} \quad (2)$$

Therefore, the inner product of the TMFs gives the commutation relation of temporal modes.

In experiments, we often treat physical quantities in finite and discrete time. For that, we define time-bin modes $\{t_j\}_{j=1}^M$ which divide time-interval $[0, T]$ into small M time bins. Their TMFs are given by

$$t_j(t) = \begin{cases} \sqrt{M/T} & [(j-1)T/M \leqslant t < jT/M], \\ 0 & \text{(otherwise)}. \end{cases} \quad (3)$$

In many cases, it is useful to use annihilation and creation operators of time-bin modes,

$$\hat{a}_{t_j} = \int dt\, t_j(t)\hat{a}(t), \quad \hat{a}_{t_j}^\dagger = \int dt\, t_j(t)\hat{a}^\dagger(t), \quad (4)$$

instead of instantaneous operators $\hat{a}(t), \hat{a}^\dagger(t)$. Their commutation relation is given by $[\hat{a}_{t_j}, \hat{a}_{t_k}^\dagger] = \delta_{j,k}$.

When $f(t)$ has finite values only in $[0, T]$ and varies slowly during the time-change T/M, it is well approximated as

$$f(t) \approx \sum_{j=1}^M f[t_j] t_j(t), \quad (5)$$

where $f[t_j] \equiv \sqrt{T/M} f(jT/M)$. Strictly speaking, both sides of Eq. (5) are not the same, but in the rest of this paper, we use an equal sign in the following for convenience:

$$f(t) = \sum_{j=1}^M f[t_j] t_j(t). \quad (6)$$

Then, by using time-bin modes, annihilation and creation operators of temporal mode f are given by

$$\hat{a}_f = \sum_{j=1}^M f^*[t_j]\hat{a}_{t_j}, \quad \hat{a}_f^\dagger = \sum_{j=1}^M f[t_j]\hat{a}_{t_j}^\dagger. \quad (7)$$

Their commutation relation is given by

$$\left[\hat{a}_{f_j}, \hat{a}_{f_k}^\dagger\right] = \sum_{l=1}^M f_j^*(t_l) f_k(t_l). \quad (8)$$

In this way, we can describe temporal mode f both in infinite-continuous time and in finite-discrete time.

When quantum states are described only by creation operators of temporal mode f and background vacuum state $|\tilde{0}\rangle$, we call them single temporal mode states in temporal mode f. Photon-number states $|n_f\rangle \equiv \frac{1}{\sqrt{n!}}(\hat{a}_f^\dagger)^n |\tilde{0}\rangle$ are the examples of such states, and they are orthogonal complete bases of single temporal mode states in temporal mode f. On the other hand, we need more than one temporal mode to describe multitemporal mode states. The basic examples are multitemporal mode Fock states $\hat{a}_{f_1}^\dagger \hat{a}_{f_2}^\dagger \cdots \hat{a}_{f_n}^\dagger |\tilde{0}\rangle$. We underline that TMFs $\{f_j(t)\}_{j=1}^n$ are arbitrary complex functions and not orthogonal to each other in general, thus we cannot describe the states as $|1_{f_1}, 1_{f_2}, \ldots, 1_{f_n}\rangle$ except for the special case when TMFs $\{f_j(t)\}_{j=1}^n$ are orthogonal functions. Our goal is to estimate the TMFs of those states by experimentally deciding the discrete values $\{f[t_j]\}_{j=1}^M$ in Eq. (6).

B. Estimation of real TMFs

Our goal is to estimate complex TMFs $f(t)$. In this section, however, we concentrate on the case where $f(t)$ are real

functions. Such functions can be estimated by applying the PCA to quadratures as introduced in Refs. [15–17]. We extend this method to the complex number in Sec. II C.

1. Data acquisition

When we try to estimate $f(t)$, one piece of useful information is quadrature values. The quadratures of instantaneous modes are defined by

$$\hat{x}_\theta(t) \equiv \frac{\hat{a}(t)e^{-i\theta} + \hat{a}^\dagger(t)e^{i\theta}}{\sqrt{2}}. \tag{9}$$

An ideal homodyne detector can measure the quadrature $\hat{x}_\theta(t)$ using a cw coherent beam called LO having a phase θ. The quadratures of a temporal mode f are given by

$$\hat{x}_{f,\theta} \equiv \frac{\hat{a}_f e^{-i\theta} + \hat{a}_f^\dagger e^{i\theta}}{\sqrt{2}} = \int dt\, f(t)\hat{x}_\theta(t). \tag{10}$$

Note that $f(t)$ is a real function here. We can obtain $\hat{x}_{f,\theta}$ by integrating the results of an ideal cw homodyne measurement with a weight $f(t)$. In the rest of the paper, we omit the suffix θ except when it is important.

In the PCA, the mode conversion of quadratures given by Eq. (10) plays a central role, thus we need a precise value of $\hat{x}(t)$. Unfortunately, homodyne detectors in laboratories are not ideal, preventing us from knowing the exact values of $\hat{x}(t)$. When the impulse response of the measurement system is given by $g(t)$, cw homodyne measurement signals are given by (under proper normalization)

$$\hat{x}'(t) = \int dt'\,\hat{x}(t')g(t - t'). \tag{11}$$

In the following, we assume $g(t)$ is mainly determined by the low-pass filter effect due to the finite bandwidth of the homodyne detector. Then, quadratures of temporal mode f we can obtain are given by

$$\hat{x}'_f \equiv \int dt\, f(t)\hat{x}'(t) = \int dt\,\hat{x}(t) \int dt'\, f(t')g(t' - t). \tag{12}$$

When $g(t)$ is narrow enough compared to $f(t)$, that is, the homodyne detector is broadband enough compared to the bandwidth of $F(\omega) \equiv \int dt\, f(t)e^{-i\omega t}$, we can regard $g(t)$ as a δ-function $\delta(t)$. It follows that:

$$\hat{x}'_f = \int dt\,\hat{x}(t)f(t) = \hat{x}_f. \tag{13}$$

Therefore, even when our homodyne detectors are not ideal, we can neglect the imperfection if they are broadband enough compared to $F(\omega)$. In the following, we express $\hat{x}'(t)$ and $\hat{x}'_f$ just as $\hat{x}(t)$ and $\hat{x}_f$ for convenience, thus $\hat{x}(t)$ and $\hat{x}_f$ means measured and calculated values by using homodyne detectors having finite but broad enough bandwidth.

In experiments, we measure quadrature values at an appropriate sampling rate during a reasonable time span. Thus, we have to treat finite and discrete time. Let us assume $f(t)$ has finite values only in time $[0, T]$. Then, we measure quadrature values M times at the same interval during $[0, T]$. Here, the sampling rate M/T should be large enough that $f(t)$ and $\hat{x}(t)$ vary slowly in time-change T/M. Note that the homodyne measurement is an observation in a system rotating at the

carrier frequency of the LO beam, thus the time changes in $f(t)$ and $\hat{x}(t)$ are not so fast. In this situation, time-bin modes $\{t_j\}_{j=1}^M$ introduced in Eq. (3) are useful. From above and Eq. (10), the quadratures of time-bin modes are given by

$$\hat{x}_{t_j} = \int dt\, t_j(t)\hat{x}(t) \approx \sqrt{T/M}\,\hat{x}(jT/M). \tag{14}$$

Similar to Eq. (6), we use an equal sign in the following:

$$\hat{x}_{t_j} = \sqrt{T/M}\,\hat{x}(jT/M). \tag{15}$$

Thus, we can determine $\hat{x}_{t_j}$ by a finite sampling rate homodyne measurement. From Eq. (7), quadratures of temporal mode f are given by

$$\hat{x}_f = \sum_{j=1}^M f[t_j]\hat{x}_{t_j}. \tag{16}$$

This equation corresponds to Eq. (10). Like above, we can define and measure quadratures both in infinite-continuous time and in finite-discrete time.

2. Principal component analysis

The PCA [18] is an analysis procedure to convert correlated variables into a set of uncorrelated variables called principal components. In the PCA, the first principal component has the largest variance in the whole space, and the following components are decided to have the largest variance in the subspace which is orthogonal to the components decided before.

In quantum optics, the PCA has been applied to the quadratures $\{\hat{x}_{t_j}\}_{j=1}^M$ to estimate real TMFs $f(t)$ of non-Gaussian states [15–17]. The variables $\{\hat{x}_{t_j}\}_{j=1}^M$ are correlated because autocorrelation functions $\langle \hat{x}_{t_j}\hat{x}_{t_k}\rangle$ are not zero in general when $j \neq k$. The PCA is a procedure to find uncorrelated variables $\{\hat{x}_{e_j}\}_{j=1}^M$ satisfying

$$\langle \hat{x}_{e_j}\hat{x}_{e_k}\rangle = \langle \hat{x}_{e_j}^2 \rangle \delta_{j,k}, \tag{17}$$

$$\langle \hat{x}_{e_1}^2 \rangle \geqslant \langle \hat{x}_{e_2}^2 \rangle \geqslant \cdots \geqslant \langle \hat{x}_{e_M}^2 \rangle. \tag{18}$$

The functions $\{e_j(t)\}_{j=1}^M$ have important information about the TMFs we want to estimate.

For example, when we apply the PCA to single-photon states $\hat{a}_f^\dagger |\tilde{0}\rangle$, we get $\langle \hat{x}_{e_1}^2 \rangle = 3/2$, $\langle \hat{x}_{e_2}^2 \rangle = \cdots = \langle \hat{x}_{e_M}^2 \rangle = 1/2$, and $f(t) = e_1(t)$ [16]. This is because single-photon states have three times larger quadrature variance than that of vacuum states in uncorrelated modes. Generally, there exists a certain phase where single temporal mode states, typically non-Gaussian states, have larger variance of quadratures than other uncorrelated vacuum modes. Therefore, $e_1(t)$ is expected to be the TMF of the single temporal mode states if we choose a proper phase of LO.

We can carry out the PCA by introducing a matrix V_t given by

$$V_t = \begin{pmatrix} \langle \hat{x}_{t_1}^2 \rangle & \langle \hat{x}_{t_1}\hat{x}_{t_2}\rangle & \cdots & \langle \hat{x}_{t_1}\hat{x}_{t_M}\rangle \\ \langle \hat{x}_{t_2}\hat{x}_{t_1}\rangle & \langle \hat{x}_{t_2}^2 \rangle & \cdots & \langle \hat{x}_{t_2}\hat{x}_{t_M}\rangle \\ \vdots & \vdots & \ddots & \vdots \\ \langle \hat{x}_{t_M}\hat{x}_{t_1}\rangle & \langle \hat{x}_{t_M}\hat{x}_{t_2}\rangle & \cdots & \langle \hat{x}_{t_M}^2 \rangle \end{pmatrix}. \tag{19}$$

We can obtain this matrix via cw homodyne measurement. When we measure a target state with a sampling rate M/T during $[0, T]$, we get a set of quadratures $\{\hat{x}_{t_j}\}_{j=1}^M$. By repeating the same measurement, we can calculate the average values $\langle \hat{x}_j \hat{x}_k \rangle$. V_t is a real symmetrical matrix thus diagonalized as $E V_t E^T$ by a certain orthogonal matrix E. In this case, such a matrix E is given by

$$E = \begin{pmatrix} e_1[t_1] & e_1[t_2] & \cdots & e_1[t_M] \\ e_2[t_1] & e_2[t_2] & \cdots & e_2[t_M] \\ \vdots & \vdots & \ddots & \vdots \\ e_M[t_1] & e_M[t_2] & \cdots & e_M[t_M] \end{pmatrix}. \quad (20)$$

Why $E V_t E^T$ is diagonalized is shown as follows. $E V_t E^T$ is given by

$$E V_t E^T = \begin{pmatrix} \langle \hat{x}_{e_1}^2 \rangle & \langle \hat{x}_{e_1} \hat{x}_{e_2} \rangle & \cdots & \langle \hat{x}_{e_1} \hat{x}_{e_M} \rangle \\ \langle \hat{x}_{e_2} \hat{x}_{e_1} \rangle & \langle \hat{x}_{e_2}^2 \rangle & \cdots & \langle \hat{x}_{e_2} \hat{x}_{e_M} \rangle \\ \vdots & \vdots & \ddots & \vdots \\ \langle \hat{x}_{e_M} \hat{x}_{e_1} \rangle & \langle \hat{x}_{e_M} \hat{x}_{e_2} \rangle & \cdots & \langle \hat{x}_{e_M}^2 \rangle \end{pmatrix}, \quad (21)$$

where we use a relation that follows from Eq. (16),

$$\langle \hat{x}_{e_j} \hat{x}_{e_k} \rangle = \sum_{l,m=1}^M e_j[t_l] e_k[t_m] \langle \hat{x}_{t_l} \hat{x}_{t_m} \rangle. \quad (22)$$

From Eq. (18), the off-diagonal terms of Eq. (21) are zero,

$$E V_t E^T = \begin{pmatrix} \langle \hat{x}_{e_1}^2 \rangle & & & \\ & \langle \hat{x}_{e_2}^2 \rangle & & 0 \\ & & \ddots & \\ 0 & & & \langle \hat{x}_{e_M}^2 \rangle \end{pmatrix}$$

$$\equiv \mathrm{diag}\big[\langle \hat{x}_{e_1}^2 \rangle, \langle \hat{x}_{e_2}^2 \rangle, \ldots, \langle \hat{x}_{e_M}^2 \rangle \big]. \quad (23)$$

In this way, we can obtain eigenfunctions $\{e_j(t)\}_{j=1}^M$ by getting matrix V_t via cw homodyne measurement and calculating a matrix E which diagonalizes V_t. Note that due to the orthogonality of E, the eigenfunctions $\{e_j(t)\}_{j=1}^M$ are orthogonal,

$$\langle e_j, e_k \rangle = \sum_{l=1}^M e_j[t_l] e_k[t_l] = \delta_{j,k}, \qquad 1 \leqslant j, \quad k \leqslant M. \quad (24)$$

Especially, in single temporal mode state analysis, TMF $f(t)$ is given by

$$f(t) = e_1(t) = \sum_{j=1}^M e_1[t_j] t_j(t) = \sum_{j=1}^M E_{1,j} t_j(t). \quad (25)$$

The PCA has been applied to experimentally created non-Gaussian states, such as single-photon states and Schrödinger's cat states in a single temporal mode [15–17]. In this method, however, the eigenfunctions $\{e_j(t)\}_{j=1}^M$ are limited to real functions because they are given by a linear combination of real functions $\{t_j(t)\}_{j=1}^M$ by orthogonal matrix E. Therefore, this method is not suitable for the quantum states which have complex TMFs. In the next section, we extend the PCA to the estimation of complex TMFs.
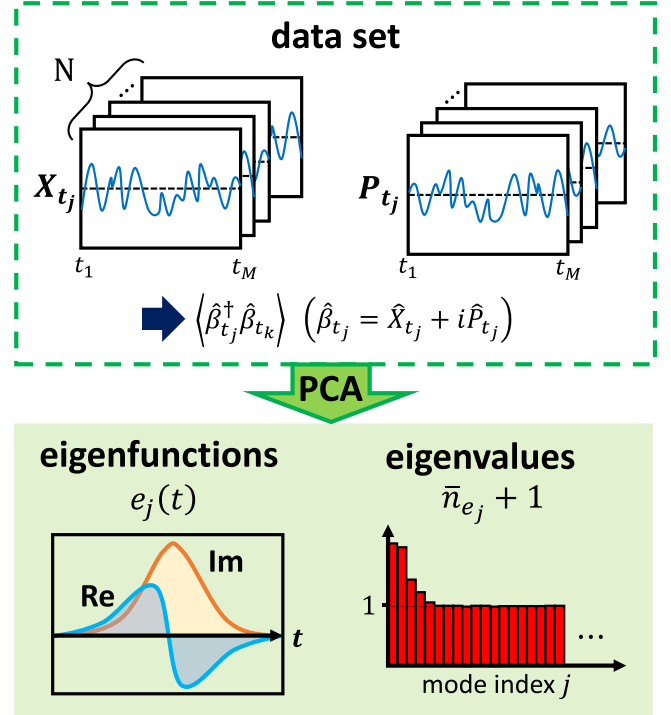

FIG. 2. Schematic of the CPCA. For every single-shot measurement, we take the quadrature values M times in $[0, T]$. We convert the complex variable $\hat{\beta}_{t_j}$ into uncorrelated variables by the PCA where we utilize the correlation $\langle \hat{\beta}_{t_j}^\dagger \hat{\beta}_{t_k} \rangle$ calculated from N-frame data. From the eigenfunctions and eigenvalues, we can estimate the TMFs of the input states.

C. Estimation of complex TMFs

1. Dual homodyne measurement

In the previous section, eigenfunctions $\{e_j(t)\}_{j=1}^M$ are limited to real functions because we apply the PCA to quadratures $\{\hat{x}_{t_j}\}_{j=1}^M$, which are real numbers. In order to estimate complex TMFs, we have to apply the PCA to complex variables. cw dual-homodyne measurement and cw heterodyne measurement give such variables, measuring the conjugate quadratures $\hat{x}_\theta(t)$ and $\hat{x}_{\theta+(\pi/2)}(t)$ simultaneously. Actually, in Ref. [19], complex TMFs of single-photon states are estimated by cw heterodyne measurement using several LOs having different frequencies. In Ref. [19], however, an optimization algorithm is adopted, requiring a heavier calculation than the PCA. In this section, we discuss applying the PCA to cw dual homodyne measurement signals. Dual homodyne can be implemented by LOs having one frequency, unlike the heterodyne method used in Ref. [19].

To begin with, we explain the cw dual homodyne measurement. Figure 2 is a conceptual diagram of the cw dual homodyne measurement. In this measurement, the target state $|\Psi\rangle$ [quadratures $\hat{x}_\theta(t)$] is divided into two outputs by a 50:50 beam splitter. Another input of the beam splitter is a vacuum state $|0\rangle$ [quadratures $\hat{x}_\theta^{(v)}(t)$]. The two outputs are measured by cw homodyne detectors by using orthogonal phases of LOs. The measurement operators of these homodynes are

given by

$$\hat{X}_{t_j} = \frac{\hat{x}_{t_j} - \hat{x}_{t_j}^{(v)}}{\sqrt{2}}, \qquad \hat{P}_{t_j} = \frac{\hat{p}_{t_j} + \hat{p}_{t_j}^{(v)}}{\sqrt{2}}, \qquad (26)$$

where we put $\hat{x} \equiv \hat{x}_{\theta=0}$, $\hat{p} \equiv \hat{x}_{\theta=\pi/2}$. We treat these values as a complex number $\hat{\beta}_{t_j}$ given by

$$\hat{\beta}_{t_j} \equiv \hat{X}_{t_j} + i\hat{P}_{t_j} = \hat{a}_{t_j} - \hat{a}_{t_j}^{\dagger(v)}. \qquad (27)$$

This value corresponds to the complex amplitude of state $|\Psi\rangle$. The vacuum term $\hat{a}_{t_j}^{\dagger(v)}$ means the uncertainty of the simultaneous measurement of $\hat{x}_{t_j}$ and $\hat{p}_{t_j}$. We define a similar value about temporal mode f as below,

$$\hat{\beta}_f \equiv \sum_{j=1}^{M} f^*[t_j]\,\hat{\beta}_{t_j} = \hat{a}_f - \hat{a}_{f^*}^{\dagger(v)}, \qquad (28)$$

$$\hat{\beta}_f^{\dagger} \equiv \sum_{j=1}^{M} f[t_j]\,\hat{\beta}_{t_j}^{\dagger} = \hat{a}_f^{\dagger} - \hat{a}_{f^*}^{(v)}. \qquad (29)$$

Note that $f(t)$ is a complex function, no longer a real function, such as in Sec. II B. The distribution of $\hat{\beta}_{f_j}$ is given by the Q function of the state in the mode f [23,24].

2. Complex-number principal component analysis

Next, let us discuss applying the PCA to the complex variables $\{\hat{\beta}_{t_j}\}_{j=1}^{M}$. This process converts correlated variables $\{\hat{\beta}_{t_j}\}_{j=1}^{M}$ into uncorrelated variables $\{\hat{\beta}_{e_j}\}_{j=1}^{M}$ which satisfy

$$\langle \hat{\beta}_{e_j}^{\dagger} \hat{\beta}_{e_k} \rangle = \langle \hat{\beta}_{e_j}^{\dagger} \hat{\beta}_{e_j} \rangle \delta_{j,k}, \qquad (30)$$

$$\langle \hat{\beta}_{e_1}^{\dagger} \hat{\beta}_{e_1} \rangle \geqslant \langle \hat{\beta}_{e_2}^{\dagger} \hat{\beta}_{e_2} \rangle \geqslant \cdots \geqslant \langle \hat{\beta}_{e_M}^{\dagger} \hat{\beta}_{e_M} \rangle. \qquad (31)$$

Let us confirm the physical meaning of the value $\langle \hat{\beta}_f^{\dagger} \hat{\beta}_f \rangle$. Equations (28) and (29) lead to

$$\hat{\beta}_f^{\dagger} \hat{\beta}_f = \hat{a}_f^{\dagger} \hat{a}_f + \hat{a}_{f^*}^{\dagger(v)} \hat{a}_{f^*}^{(v)} + 1 - \hat{a}_f^{\dagger} \hat{a}_{f^*}^{\dagger(v)} - \hat{a}_f \hat{a}_{f^*}^{(v)}. \qquad (32)$$

Because the cw dual homodyne measurement has two-mode input $|\Psi\rangle |0_v\rangle$, the average value is given by

$$\begin{aligned} \langle \hat{\beta}_f^{\dagger} \hat{\beta}_f \rangle &= \langle 0_v| \langle \Psi| \hat{\beta}_f^{\dagger} \hat{\beta}_f |\Psi\rangle |0_v\rangle \\ &= \langle \Psi| \hat{a}_f^{\dagger} \hat{a}_f |\Psi\rangle + 1 \\ &\equiv \bar{n}_f + 1. \end{aligned} \qquad (33)$$

Therefore, $\langle \hat{\beta}_f^{\dagger} \hat{\beta}_f \rangle$ shows the average photon number state $|\Psi\rangle$ has in a temporal mode f. For example, when applying the PCA to single-photon states $\hat{a}_f^{\dagger} |\tilde{0}\rangle$, we get $\bar{n}_{e_1} = 1$, $\bar{n}_{e_2} = \cdots = \bar{n}_{e_M} = 0$, and $e_1(t) = f(t)$. Generally, when we analyze single temporal mode states, only $\bar{n}_{e_1}$ is larger than zero, and $e_1(t) = f(t)$. To distinguish from the previous PCA, we call this method the CPCA in this paper.

We can carry out the CPCA by introducing a matrix C_t given by

$$C_t = \begin{pmatrix} \langle \hat{\beta}_{t_1}^{\dagger} \hat{\beta}_{t_1} \rangle & \langle \hat{\beta}_{t_1}^{\dagger} \hat{\beta}_{t_2} \rangle & \cdots & \langle \hat{\beta}_{t_1}^{\dagger} \hat{\beta}_{t_M} \rangle \\ \langle \hat{\beta}_{t_2}^{\dagger} \hat{\beta}_{t_1} \rangle & \langle \hat{\beta}_{t_2}^{\dagger} \hat{\beta}_{t_2} \rangle & \cdots & \langle \hat{\beta}_{t_2}^{\dagger} \hat{\beta}_{t_M} \rangle \\ \vdots & \vdots & \ddots & \vdots \\ \langle \hat{\beta}_{t_M}^{\dagger} \hat{\beta}_{t_1} \rangle & \langle \hat{\beta}_{t_M}^{\dagger} \hat{\beta}_{t_2} \rangle & \cdots & \langle \hat{\beta}_{t_M}^{\dagger} \hat{\beta}_{t_M} \rangle \end{pmatrix}. \qquad (34)$$

We can obtain this matrix via a cw dual homodyne measurement. We measure a target state with a sampling rate M/T during $[0, T]$ to get a set of values $\{\hat{\beta}_{t_j}\}_{j=1}^{M}$. By repeating the same measurement, we can calculate $\langle \hat{\beta}_{t_j}^{\dagger} \hat{\beta}_{t_k} \rangle$. C_t is a Hermite matrix thus diagonalized by a unitary matrix E as follows:

$$E = \begin{pmatrix} e_1[t_1] & e_1[t_2] & \cdots & e_1[t_M] \\ e_2[t_1] & e_2[t_2] & \cdots & e_2[t_M] \\ \vdots & \vdots & \ddots & \vdots \\ e_M[t_1] & e_M[t_2] & \cdots & e_M[t_M] \end{pmatrix}, \qquad (35)$$

$$EC_t E^{\dagger} = \mathrm{diag}\big[\langle \hat{\beta}_{e_1}^{\dagger} \hat{\beta}_{e_1} \rangle, \langle \hat{\beta}_{e_2}^{\dagger} \hat{\beta}_{e_2} \rangle, \ldots, \langle \hat{\beta}_{e_M}^{\dagger} \hat{\beta}_{e_M} \rangle\big]$$

$$= \mathrm{diag}\big[\bar{n}_{e_1} + 1, \bar{n}_{e_2} + 1, \ldots, \bar{n}_{e_M} + 1\big]. \qquad (36)$$

In the diagonalization of C_t, we use a relation derived from Eqs. (28) and (29),

$$\langle \hat{\beta}_{e_j}^{\dagger} \hat{\beta}_{e_k} \rangle = \sum_{l,m=1}^{M} e_j[t_l] e_k^*[t_m] \langle \hat{\beta}_{t_l}^{\dagger} \hat{\beta}_{t_m} \rangle. \qquad (37)$$

Like the PCA, we can obtain eigenfunctions $\{e_j(t)\}_{j=1}^{M}$ and average photon-numbers $\{\bar{n}_{e_j}\}_{j=1}^{M}$ through the diagonalizing process. The important thing is that eigenfunctions $\{e_j(t)\}_{j=1}^{M}$ are complex functions because the matrix E is unitary. It also follows:

$$\langle e_j, e_k \rangle = \delta_{j,k}, \qquad 1 \leqslant j, \quad k \leqslant M. \qquad (38)$$

In single temporal mode state analysis, the TMF $f(t)$ is given by

$$f(t) = e_1(t) = \sum_{j=1}^{M} e_1[t_j], \qquad t_j(t) = \sum_{j=1}^{M} E_{1,j} t_j(t). \qquad (39)$$

Like above, we can estimate the complex TMF of single temporal mode states via the CPCA.

D. Dual temporal mode state analysis

In the previous section, we discussed single temporal mode state analysis by the CPCA. However, useful states are often defined in multitemporal modes. For example, some quantum error correction codes use multimode states to protect fragile quantum information [20–22]. Therefore, we should develop mode characterization tools for multimode states. As a simple case, we treat two photons distributed in two temporal modes. As shown in Ref. [8], such states always can be given by

$$|\Psi_2\rangle = \frac{1}{\sqrt{1 + |\langle f_1, f_2 \rangle|^2}} \hat{a}_{f_1}^{\dagger} \hat{a}_{f_2}^{\dagger} |\tilde{0}\rangle, \qquad (40)$$

where $f_1(t)$, $f_2(t)$ are complex functions not orthogonal in general. We will characterize the temporal mode structures of $|\Psi_2\rangle$ by estimating $f_1(t)$ and $f_2(t)$. In the following, we assume $f_1(t) \neq f_2(t)$.

When we apply the CPCA to $|\Psi_2\rangle$, $\bar{n}_{e_2}$ is no longer zero but has a positive value. Thus, e_1 and e_2 have the information of the temporal mode structures of $|\Psi_2\rangle$. From Eq. (38), modes e_1 and e_2 are orthogonal. Note that in most cases e_1, e_2 are not the same modes as f_1, f_2 because f_1, f_2 are not orthogonal in general. The two photons in $|\Psi_2\rangle$ are distributed in e_1, e_2, thus

$|\Psi_2\rangle$ can be described by

$$|\Psi_2\rangle = \alpha\,|2_{e_1}, 0_{e_2}\rangle + \beta\,|1_{e_1}, 1_{e_2}\rangle + \gamma\,|0_{e_1}, 2_{e_2}\rangle$$

$$= \left(\frac{\alpha}{\sqrt{2}}\hat{a}_{e_1}^{\dagger\,2} + \beta\,\hat{a}_{e_1}^{\dagger}\hat{a}_{e_2}^{\dagger} + \frac{\gamma}{\sqrt{2}}\hat{a}_{e_2}^{\dagger\,2}\right)|\tilde{0}\rangle, \quad (41)$$

where $\alpha \in \mathbb{R}$ and $\beta, \gamma \in \mathbb{C}$ satisfy $\alpha^2 + |\beta|^2 + |\gamma|^2 = 1$. The quadratic polynomial of the creation operators in Eq. (41) can be decomposed into a product of linear polynomials,

$$|\Psi_2\rangle = \frac{\left(d_{11}\hat{a}_{e_1}^{\dagger} + d_{12}\hat{a}_{e_2}^{\dagger}\right)\left(d_{21}\hat{a}_{e_1}^{\dagger} + d_{22}\hat{a}_{e_2}^{\dagger}\right)}{\sqrt{1 + |d_{11}^* d_{21} + d_{12}^* d_{22}|^2}}|\tilde{0}\rangle, \quad (42)$$

where $|d_{11}|^2 + |d_{12}|^2 = 1$, $|d_{21}|^2 + |d_{22}|^2 = 1$. From Eq. (1), we can use the next relation for arbitrary normalized orthogonal functions $g_1(t)$ and $g_2(t)$,

$$\eta_1\hat{a}_{g_1}^{\dagger} + \eta_2\hat{a}_{g_2}^{\dagger} = \hat{a}_{\eta_1 g_1 + \eta_2 g_2}^{\dagger} \quad (|\eta_1|^2 + |\eta_2|^2 = 1). \quad (43)$$

Thus, we can get

$$|\Psi_2\rangle = \frac{1}{\sqrt{1 + |d_{11}^* d_{21} + d_{12}^* d_{22}|^2}}\hat{a}_{d_{11}e_1 + d_{12}e_2}^{\dagger}\hat{a}_{d_{21}e_1 + d_{22}e_2}^{\dagger}|\tilde{0}\rangle.$$

$$(44)$$

This is the same form as Eq. (40), thus $f_1(t)$, $f_2(t)$ are given by

$$\begin{pmatrix} f_1(t) \\ f_2(t) \end{pmatrix} = \begin{pmatrix} d_{11} & d_{12} \\ d_{21} & d_{22} \end{pmatrix}\begin{pmatrix} e_1(t) \\ e_2(t) \end{pmatrix} \equiv D\begin{pmatrix} e_1(t) \\ e_2(t) \end{pmatrix}. \quad (45)$$

Our goal is to calculate $f_1(t)$ and $f_2(t)$ experimentally. We can get $e_1(t)$, $e_2(t)$ by the CPCA, thus we express the matrix D by experimentally obtainable values.

By assuming $d_{11}, d_{21} \in \mathbb{R}$, we can determine D uniquely from α, β, and γ. From Eqs. (33) and (41), these values should satisfy

$$\bar{n}_{e_1} = \langle\Psi_2|\hat{\beta}_{e_1}^{\dagger}\hat{\beta}_{e_1}|\Psi_2\rangle - 1 = 2\alpha^2 + |\beta|^2,$$

$$\bar{n}_{e_2} = \langle\Psi_2|\hat{\beta}_{e_2}^{\dagger}\hat{\beta}_{e_2}|\Psi_2\rangle - 1 = |\beta|^2 + 2|\gamma|^2, \quad (46)$$

$$0 = \langle\Psi_2|\hat{\beta}_{e_1}^{\dagger}\hat{\beta}_{e_2}|\Psi_2\rangle = \sqrt{2}(\alpha\beta + \beta^*\gamma).$$

Thus, when $\bar{n}_1 > \bar{n}_2 > 0$,

$$\alpha = \sqrt{\frac{\bar{n}_1}{2}}, \qquad \beta = 0, \qquad |\gamma| = \sqrt{\frac{\bar{n}_2}{2}}. \quad (47)$$

When $\bar{n}_1 = \bar{n}_2 = 1$,

$$\alpha = |\gamma| = \sqrt{\frac{1 - |\beta|^2}{2}}, \qquad 2\arg\beta = \arg\gamma \pm \pi. \quad (48)$$

There still exists uncertainty among α, β, and γ. Therefore, we cannot decide D only from the CPCA results.

Interestingly, we can overcome this problem by introducing fourth-order moments. First, we utilize

$$qe^{i\theta} \equiv \langle\Psi_2|\hat{\beta}_{e_1}^{\dagger 2}\hat{\beta}_{e_2}^2|\Psi_2\rangle = 2\alpha\gamma \qquad (q \geqslant 0). \quad (49)$$

You can easily obtain this value experimentally because you have the data set $\{\hat{\beta}_{t_j}\}_{j=1}^{M}$ and eigenfunctions $e_1(t)$, $e_2(t)$ to calculate the values $\hat{\beta}_{e_1}^{\dagger}$, $\hat{\beta}_{e_2}$ using Eqs. (28) and (29). Equation (49) leads to

$$2\alpha|\gamma| = q, \qquad \arg\gamma = \theta. \quad (50)$$

From Eqs. (47), (48), and (50), we can determine α, β, and γ, thus the matrix D. When $\bar{n}_1 > \bar{n}_2 > 0$,

$$\alpha = \sqrt{\frac{\bar{n}_1}{2}}, \qquad \beta = 0, \qquad \gamma = \sqrt{\frac{\bar{n}_2}{2}}e^{i\theta} \quad (51)$$

$$D = \frac{1}{\sqrt{\bar{n}_{e_1}^{1/2} + \bar{n}_{e_2}^{1/2}}}\begin{pmatrix} \bar{n}_{e_1}^{1/4} & i\bar{n}_{e_2}^{1/4}e^{i(\theta/2)} \\ \bar{n}_{e_1}^{1/4} & -i\bar{n}_{e_2}^{1/4}e^{i(\theta/2)} \end{pmatrix}. \quad (52)$$

When $\bar{n}_1 = \bar{n}_2 = 1$,

$$\alpha = \sqrt{\frac{q}{2}}, \qquad \beta = \pm i\sqrt{1-q}e^{i(\theta/2)}, \qquad \gamma = \sqrt{\frac{q}{2}}e^{i\theta}$$

$$(53)$$

$$D = \begin{pmatrix} \sqrt{1 + \sqrt{1-q}} & \mp i\sqrt{1 - \sqrt{1-q}}e^{i(\theta/2)} \\ \sqrt{1 - \sqrt{1-q}} & \pm i\sqrt{1 + \sqrt{1-q}}e^{i(\theta/2)} \end{pmatrix}. \quad (54)$$

The latter case corresponds to the situation when f_1 and f_2 are orthogonal because the columns of D are orthogonal. In this case, the phase of β is still not unique. We can determine the phase by using another fourth-order moment $\langle\Psi_2|\hat{\beta}_{e_1}^{\dagger 2}\hat{\beta}_{e_1}\hat{\beta}_{e_2}|\Psi_2\rangle = 2\alpha\beta$, which reveals $\arg\beta$.

In this way, we can characterize the temporal mode structures of $|\Psi_2\rangle$ experimentally. What we have to do is executing the CPCA to obtain $e_1(t)$, $e_2(t)$, $\bar{n}_{e_1}$, and $\bar{n}_{e_2}$ and calculating the fourth-order moments from the dual homodyne signals and $e_1(t)$, $e_2(t)$. Then, following Eqs. (45) and (52) or (54), we can calculate $f_1(t)$ and $f_2(t)$ in Eq. (40). In the next section, we will discuss the case when the analysis objects have errors due to a lossy optical channel.

E. Effect of photon loss

We discussed pure states so far. In experiment, however, what we can prepare is mixed states due to the coupling between quantum states and the environment. Usually, the most dominant error is photon loss. In this section, we show that the analysis method discussed in Secs. II C and II D can work even when photon loss exists.

When we treat pure states $|\Psi\rangle$, the (j, k) component of C_t is given by

$$C_{t,jk}(|\Psi\rangle\langle\Psi|) = \langle\Psi|\hat{\beta}_{t_j}^{\dagger}\hat{\beta}_{t_k}|\Psi\rangle = \langle\Psi|\hat{a}_{t_j}^{\dagger}\hat{a}_{t_k}|\Psi\rangle + \delta_{j,k}.$$

$$(55)$$

The photon loss process is usually described by a beam-splitter model. When one photon is lost with a probability p, the mode $\hat{a}_f$ is mixed with a vacuum mode $\hat{a}_f^{(v)}$ by a beam splitter whose transmittance is $1 - p$ $(0 < p < 1)$,

$$\hat{A}_f = \sqrt{1-p}\hat{a}_f + \sqrt{p}\hat{a}_f^{(v)}. \quad (56)$$

Similarly, $\hat{\beta}_f$ in Eq. (28) is changed into $\hat{B}_f$ given by

$$\hat{B}_f = \sqrt{1-p}\hat{a}_f + \sqrt{p}\hat{a}_f^{(v1)} - \hat{a}_{f^*}^{\dagger(v2)}, \quad (57)$$

where $\hat{a}_f^{(v1)}$ and $\hat{a}_{f^*}^{\dagger(v2)}$ are vacuum terms due to the photon loss and dual homodyne measurement. Photon loss degrades pure states $|\Psi\rangle$ into mixed states $\hat{\rho}$, then the (j, k) component of C_t

in Eq. (34) is given by

$$
\begin{aligned}
C_{t,jk}(\hat{\rho}) &= \mathrm{tr}\big[\hat{\rho}\hat{B}_{t_j}^{\dagger}\hat{B}_{t_k}\big] \\
&= \langle 0_{v_1}|\,\langle 0_{v_2}|\,\langle\Psi|\hat{B}_{t_j}^{\dagger}\hat{B}_{t_k}|\Psi\rangle\,|0_{v_1}\rangle\,|0_{v_2}\rangle \\
&= (1-p)\langle\Psi|\hat{a}_{t_j}^{\dagger}\hat{a}_{t_k}|\Psi\rangle + \delta_{j,k}\,.
\end{aligned}
\tag{58}
$$

Thus, we get

$$
C_t(\hat{\rho}) = (1-p)C_t(|\Phi\rangle\langle\Phi|) + pI,
\tag{59}
$$

where I is an M-dimensional identity matrix. When $C_t(|\Psi\rangle\langle\Psi|)$ is diagonalized by E, such as Eq. (36), $C_t(\hat{\rho})$ is also diagonalized by E as follows:

$$
\begin{aligned}
EC_t(\hat{\rho})E^{\dagger} &= \mathrm{diag}\big[(1-p)\bar{n}_{e_1}+1,\ldots,(1-p)\bar{n}_{e_M}+1\big] \\
&\equiv \mathrm{diag}\big[\bar{N}_{e_1}+1,\ldots,\bar{N}_{e_M}+1\big].
\end{aligned}
\tag{60}
$$

Therefore, photon loss only changes $\{\bar{n}_{e_j}\}_{j=1}^{M}$ into $\{\bar{N}_{e_j}\}_{j=1}^{M}$, and we can assume the CPCA gives the same eigenfunctions $\{e_j(t)\}_{j=1}^{M}$ in the pure state case and mixed state case.

Let us discuss how photon loss affects our analysis method. In single temporal mode state analysis, what we want is the eigenfunction $e_1(t)$ as explained in Sec. II C, thus photon loss does not affect the analysis procedure.

In Sec. II D, we calculated $f_1(t)$, $f_2(t)$ from $e_1(t)$, $e_2(t)$ and matrix D given by Eqs. (52) and (54). We can still obtain $e_1(t)$, $e_2(t)$, but we need a slight modification about D. We introduced a fourth-order moment $qe^{i\theta}$ in Eq. (49). When photon loss exists, what we actually obtain is given by

$$
q'e^{i\Theta} \equiv \mathrm{tr}\big[\hat{\rho}\hat{B}_{e_1}^{\dagger\,2}\hat{B}_{e_2}^{2}\big] = (1-p)^2qe^{i\theta}.
\tag{61}
$$

Thus, the phase of the moment is not affected. Because $\bar{N}_{e_1} + \bar{N}_{e_2} = 2(1-p)$, we can modify the norm of the moment,

$$
Q \equiv \frac{4q'}{\big(\bar{N}_{e_1}+\bar{N}_{e_2}\big)^2}.
\tag{62}
$$

Then, Eqs. (52) and (54) are modified as follows:

$$
D = \frac{1}{\sqrt{\bar{N}_{e_1}^{1/2}+\bar{N}_{e_2}^{1/2}}}\begin{pmatrix} \bar{N}_{e_1}^{1/4} & i\bar{N}_{e_2}^{1/4}e^{(i/2)\Theta} \\ \bar{N}_{e_1}^{1/4} & -i\bar{N}_{e_2}^{1/4}e^{(i/2)\Theta} \end{pmatrix},
\tag{63}
$$

$$
D = \begin{pmatrix} \sqrt{1+\sqrt{1-Q}} & \mp i\sqrt{1-\sqrt{1-Q}}\,e^{i(\Theta/2)} \\ \sqrt{1-\sqrt{1-Q}} & \pm i\sqrt{1+\sqrt{1-Q}}\,e^{i(\Theta/2)} \end{pmatrix}.
\tag{64}
$$

We can decide the sign of Eq. (64) by the phase of another moment $\mathrm{tr}[\hat{\rho}\hat{B}_{e_1}^{\dagger 2}\hat{B}_{e_1}\hat{B}_{e_2}]$, which is also not affected by photon loss. Therefore, we can calculate the functions $f_1(t)$, $f_2(t)$ experimentally even when photon loss exists.

In this section, we showed photon loss does not affect our TMF estimation essentially. In the next section, we briefly summarize which states can be analyzed by the CPCA and which states cannot be.

F. Application range of the CPCA

Here, we summarize the application range of the CPCA. This method can deal with arbitrary non-Gaussian states in arbitrary single temporal modes. Note that we assume vacuum states exist in all temporal modes orthogonal to the ones in which the target non-Gaussian states exist. The analyzed

states can be mixed states, and the TMFs are not limited to real functions. The CPCA can also deal with arbitrary two-photon states where each photon occupies a single temporal mode. We can remove the effect of photon loss when we analyze these states.

Note that there still exist many hurdles for analysis of general multitemporal mode states. As an example, let us consider dual temporal mode states described by TMFs $f_1(t)$ and $f_2(t)$. Here, these TMFs are arbitrary complex functions not orthogonal in general. In Secs. II D and II E, we showed how to estimate $f_1(t)$ and $f_2(t)$ of two-photon states $\hat{a}_{f_1}^{\dagger}\hat{a}_{f_2}^{\dagger}|\tilde{0}\rangle$. Unfortunately, the same calculation cannot be applied to other dual temporal mode states, such as mixed states $\frac{1}{2}\hat{a}_{f_1}^{\dagger}|\tilde{0}\rangle\langle\tilde{0}|\hat{a}_{f_1} + \frac{1}{2}\hat{a}_{f_2}^{\dagger}|\tilde{0}\rangle\langle\tilde{0}|\hat{a}_{f_2}$ or entangled states $\hat{a}_{f_1}^{\dagger}|\tilde{0}\rangle + \hat{a}_{f_2}^{\dagger}|\tilde{0}\rangle + \hat{a}_{f_1}^{\dagger}\hat{a}_{f_2}^{\dagger}|\tilde{0}\rangle$. Another example is multitemporal mode Fock states $|\Psi_n\rangle \propto \hat{a}_{f_1}\hat{a}_{f_2}\cdots\hat{a}_{f_n}|\tilde{0}\rangle$, where $f_1(t), f_2(t), \ldots, f_n(t)$ are arbitrary complex functions not orthogonal in general. When $n=2$ we can estimate $f_1(t)$ and $f_2(t)$ by solving Eqs. (47) and (50). In principle, a similar estimation can be applied to $|\Psi_n\rangle$, however, it becomes difficult as n increases to analytically solve this problem. Temporal mode characterization of these general multitemporal mode states is still a future work.

In the next section, we demonstrate these methods.

III. EXPERIMENT

A. Heralded creation of optical non-Gaussian states

High-purity non-Gaussian states have been created by a heralded scheme [25–30]. In this method, entangled two modes (idler and signal modes) are prepared, and photon detection in the idler mode heralds non-Gaussian states in the signal mode. So far, such states as single-photon states, superposition of photon-number states, and Schrödinger's cat states have been created [25–30]. These created states are defined in wave-packet temporal modes, called time-bin modes. The envelopes of the wave packets give the TMF of the modes.

In this scheme, we can engineer the TMFs by the configuration of the idler path. Especially, the TMFs can be complex when we put an asymmetric Mach-Zehnder interferometer in an idler path [11]. Therefore, the heralded creation of non-Gaussian states using interferometers is a good way to demonstrate the CPCA. To verify our temporal mode estimation method, we conduct three types of heralding experiments with an interferometer. The first one is the analysis of the time-bin qubit as the simplest example. The second one is the analysis of what we call the *dual-rail cat qubit*, a qubit consisting of Schrödinger's cat states. This experiment shows our method's ability to deal with phase-sensitive and multiphoton states in a single temporal mode. The last one is the analysis of a time-bin qutrit containing two photons to verify our dual temporal mode analysis explained in Sec. II D. In the following, we explain how these qubits and qutrits are related to our complex TMF estimation method.

The generation of time-bin qubits and qutrits has already been realized in Refs. [8,11]. In those studies, the idler and signal modes are realized by a two-mode squeezed vacuum emitted from the nondegenerate optical parametric oscillator (OPO). One- (two-) photon detection after interferometer(s)

in the idler mode heralds time-bin qubits (qutrits) in the signal mode. Time-bin qubits [11] are generally recognized as two temporal mode states where one photon is distributed in two orthogonal time-bin modes w_1 and w_2. They are described as $p_1 |1_{w_1}\rangle + p_2 |1_{w_2}\rangle \equiv p_1 |1_{w_1}, 0_{w_2}\rangle + p_2 |0_{w_1}, 1_{w_2}\rangle$. Here, the TMFs $w_1(t)$ and $w_2(t)$ are real functions, such as in Ref. [16]. By using Eq. (43), these states are transformed as

$$p_1 |1_{w_1}, 0_{w_2}\rangle + p_2 |0_{w_1}, 1_{w_2}\rangle = (p_1 \hat{a}_{w_1}^\dagger + p_2 \hat{a}_{w_2}^\dagger) |\tilde{0}\rangle$$
$$= \hat{a}_{p_1 w_1 + p_2 w_2}^\dagger |\tilde{0}\rangle . \quad (65)$$

Thus time-bin qubits are single temporal mode single-photon states, whose TMFs $p_1 w_1(t) + p_2 w_2(t)$ are complex functions because $p_1, p_2 \in \mathbb{C}$. The CPCA can estimate this kind of complex TMFs.

Similarly, time-bin qutrits [8], two photons distributed in w_1 and w_2, are described as

$$q_1 |2_{w_1}, 0_{w_2}\rangle + q_2 |1_{w_1}, 1_{w_2}\rangle + q_3 |0_{w_1}, 2_{w_2}\rangle$$
$$= \frac{1}{\sqrt{1 + |r_1^* r_3 + r_2^* r_4|^2}} \hat{a}_{r_1 w_1 + r_2 w_2}^\dagger \hat{a}_{r_3 w_1 + r_4 w_2}^\dagger |\tilde{0}\rangle , \quad (66)$$

as explained in Sec. II D. Equation (66) has the same form as Eq. (40), thus we can estimate $f_1(t) = r_1 w_1(t) + r_2 w_2(t)$ and $f_2(t) = r_3 w_1(t) + r_4 w_2(t)$, both are the complex functions. We can decide the coefficients p_1, p_2 and r_1, r_2, r_3, and r_4 arbitrarily by changing the power ratio and relative phase of the beams in two arms of the interferometer.

On top of that, we generate dual-rail cat qubits by the heralded scheme. Here, the signal mode is a one-mode squeezed vacuum emitted from a degenerate OPO. The idler mode is weakly tapped from the signal mode by a beam splitter. We use the same interferometer as time-bin qubit experiments in the idler path. One-photon detection in the idler mode is recognized as a photon subtraction from the squeezed vacuum, thus the state heralded in the signal mode is given by

$$(s_1 \hat{a}_{w_1} + s_2 \hat{a}_{w_2}) \hat{S}_r(w_1) \hat{S}_r(w_2) |\tilde{0}\rangle , \quad (67)$$

where a squeezing operator of a temporal mode f is given by

$$\hat{S}_r(f) = \exp \frac{r}{2} (\hat{a}_f^{\dagger 2} - \hat{a}_f^2). \quad (68)$$

Note that, in Eq. (67), the squeezing operation in the temporal modes orthogonal to w_1 and w_2 is ignored for simplicity. By choosing proper r, the photon-subtracted squeezed state becomes very similar to a Schrödinger's cat state [28]. Thus, Eq. (67) is a qubit described by

$$s_1 |\text{Cat}_{w_1}, \text{Squeeze}_{w_2}\rangle + s_2 |\text{Squeeze}_{w_1}, \text{Cat}_{w_2}\rangle . \quad (69)$$

Note that the basis states of the qubits are orthogonal because cat states (squeezed states) have only odd (even) photon-number components. We can decide $s_1, s_2 \in \mathbb{C}$ by the interferometer arbitrarily in the same way as the time-bin qubits' case. For example, when $s_1 = s_2 = 1/\sqrt{2}$, Eq. (67) is given by

$$\hat{a}_{[(w_1 + w_2)/\sqrt{2}]} \hat{S}_r\left(\frac{w_1 + w_2}{\sqrt{2}}\right) \hat{S}_r\left(\frac{w_1 - w_2}{\sqrt{2}}\right) |\tilde{0}\rangle . \quad (70)$$

Thus, it is a single temporal mode Schrödinger's cat state in $(w_1 + w_2)/\sqrt{2}$. Similar mode transformation of the squeezed

operation is seen in Ref. [31]. On the other hand, when we consider complex temporal modes, we need to introduce a two-mode squeezing operator. When $s_1 = 1/\sqrt{2}$, $s_2 = -i/\sqrt{2}$, Eq. (67) is

$$\hat{a}_{[(w_1 - iw_2)/\sqrt{2}]} \hat{S}_r^{(2)}\left(\frac{w_1 + iw_2}{\sqrt{2}}, \frac{w_1 - iw_2}{\sqrt{2}}\right) |\tilde{0}\rangle , \quad (71)$$

where a two-mode squeezing operator of orthogonal modes f_1, f_2 is given by

$$\hat{S}_r^{(2)}(f_1, f_2) = \exp r(\hat{a}_{f_1}^\dagger \hat{a}_{f_2}^\dagger - \hat{a}_{f_1} \hat{a}_{f_2}). \quad (72)$$

In the photon-number basis, Eq. (71) is given by [32]

$$\hat{a}_{[(w_1 - iw_2/\sqrt{2})]} \frac{1}{\cosh r} \sum_{n=0}^\infty (\tanh r)^n$$
$$\left| n_{[(w_1 + iw_2)/\sqrt{2}]}, n_{[(w_1 - iw_2)/\sqrt{2}]} \right\rangle$$
$$= \frac{1}{\cosh r} \sum_{n=0}^\infty \sqrt{n+1} (\tanh r)^{n+1}$$
$$\left| n + 1_{[(w_1 + iw_2)/\sqrt{2}]}, n_{[(w_1 - iw_2)/\sqrt{2}]} \right\rangle . \quad (73)$$

When $r \to \infty$, the created state is a photon-subtracted Einstein-Podolsky-Rosen (EPR) state. Subtraction makes the average photon number larger in $(w_1 - iw_2)/\sqrt{2}$ and especially in $(w_1 + iw_2)/\sqrt{2}$. This is a kind of entanglement purification similar to Ref. [33].

The modes $(w_1 + iw_2)/\sqrt{2}$ and $(w_1 - iw_2)/\sqrt{2}$ are orthogonal and satisfy

$$\langle \hat{\beta}_{[(w_1 + iw_2)/\sqrt{2}]}^\dagger \hat{\beta}_{[(w_1 - iw_2)/\sqrt{2}]} \rangle$$
$$= \langle \hat{\beta}_{[(w_1 - iw_2)/\sqrt{2}]}^\dagger \hat{\beta}_{[(w_1 + iw_2)/\sqrt{2}]} \rangle = 0. \quad (74)$$

Therefore, it is expected that the CPCA gives $e_1(t) = [w_1(t) + iw_2(t)]/\sqrt{2}$ and $e_2(t) = [w_1(t) - iw_2(t)]/\sqrt{2}$.

B. Experimental setup

The schematic of time-bin qubit and qutrit generation is shown in Fig. 3. This setup is the same as Refs. [8,11]. The light source of the experiment is a cw Ti:sapphire laser whose wavelength is 860 nm. A bow tie-shaped nondegenerate OPO is used to generate two-mode squeezed vacuum states. The cavity of the OPO has 16 MHz of full width at half maximum and 600 MHz of free spectrum range (FSR). Inside the cavity, a 10-mm length periodically poled $KTiOPO_4$ crystal is placed as a nonlinear optical medium. The pump beam of the OPO is produced from a SHG, which consists of a bow tie-shaped cavity and a 10-mm length $KNbO_3$ crystal. The pump beam is given a 600-MHz (one FSR) frequency shift by an AOM.

Signal and idler modes of the two-mode squeezed vacuum states have different frequencies and are divided into two optical paths by a splitting cavity. The idler mode passes through two Fabry-Pérot filter cavities to filter out unwanted nondegenerate modes. When the OPO is weakly pumped, photon detection by a silicon APD in the idler mode heralds single-photon states in the signal mode. In order to create time-bin qubits, we construct an asymmetric Mach-Zehnder interferometer between the filter cavities and the APD. The idler field in the longer arm of the interferometer is a given
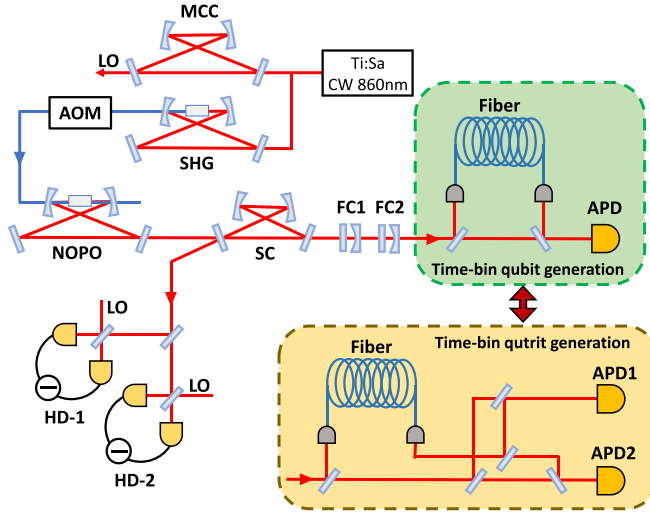
FIG. 3. Experimental setup for the heralded creation of time-bin qubits $p_1 |1_{w_1}, 0_{w_2}\rangle + p_2 |0_{w_1}, 1_{w_2}\rangle$ and time-bin qutrits $q_1 |2_{w_1}, 0_{w_2}\rangle + q_2 |1_{w_1}, 1_{w_2}\rangle + q_2 |0_{w_1}, 2_{w_2}\rangle$. Ti:sapphire denotes a titanium sapphire laser, second-harmonic generator (SHG), mode cleaning cavity (MCC), acousto-optical modulator (AOM), nondegenerate optical prametric oscillator (NOPO), splitting cavity (SC), filter cavity (FC), avalanche photodiode (APD), LO, and homodyne detector (HD). In the photon-subtraction experiments, the AOM is removed, and the SC is replaced by a 97% reflection beam splitter in the time-bin qubit generation setup.

time delay against the idler field in the shorter arm, thus time-shifted idler fields interfere before photon detection. This interference enables the photon detection by an APD to herald time-bin superposition states. The longer arm of the interferometer is implemented by an about a 50-m optical fiber, which is long enough to regard the heralded two time bins as orthogonal. Arbitrary time-bin qubits can be created by changing the power ratio and relative phase of two beams in the interferometer. In the case of the creation of time-bin qutrits, we combine two asymmetric Mach-Zehnder interferometers and two APDs. In this case, simultaneous photon detection at two APDs heralds time-bin qutrits in the signal mode.

In dual-rail cat qubit generation, we remove the AOM to use the OPO as a degenerate OPO to generate one-mode squeezed vacuum. The splitting cavity is replaced by a 97% reflection beam splitter. The interferometer in the idler path is same as the time-bin qubit setup. We generate single temporal mode Schrödinger's cat states and photon-subtracted EPR states by changing the relative phase of the beams in the two arms of the interferometer.

All these created states are detected by the cw dual homodyne measurement. The transversal mode of the LO beams for the homodyne measurement is set to TEM$_{00}$ by a bow tie-shaped mode cleaning cavity. The sampling rate of data acquisition is 1 GHz, and one data frame contains 1500 points ($T = 1.5\ \mu$s, $M = 1500$). Each state is measured 20 000 times to construct the matrix C_t introduced in Eq. (34). In this case, C_t is a (1500 × 1500)-dimensional matrix. Measured values are filtered by a second-order LC high-pass filter and a digital low-pass filter to filter out the effect of high

signal noise at dc and gain peaking of homodyne detectors at high frequencies. The cutoff frequencies are 100 kHz and 14.3 MHz, respectively.

Theoretically, the time-bin TMF has the double-decaying exponential profile $\sqrt{\gamma} e^{-\gamma|t|}$ where $\gamma = 1.1 \times 10^8$/s is a Fourier counterpart of OPO's Lorentzian frequency spectrum [12]. The low-pass filter effect of two filter cavities and a digital filter make the actual TMF $w(t)$ to be round shaped [34]. On top of that, a 50-m optical fiber makes time-shifted superposition of two time-bin modes $w_1(t)$ and $w_2(t)$, where $w_2(t) = w_1(t - \Delta t)$, $\Delta t \approx 250$ ns. This time delay is enough to assume that these two modes are orthogonal, considering the exponential decay of the function $w(t)$ given by γ. We estimate the mode functions seen in Eqs. (65) and (66), thus experimental results are expected to be superposition of $w_1(t)$ and $w_2(t)$ as you can see in the next section.

C. Results

1. Time-bin qubit and dual-rail cat qubit

We show the analysis results of two types of time-bin qubits given by

$$|\phi_1\rangle = \frac{1}{\sqrt{2}} \left(|1_{w_1}, 0_{w_2}\rangle + |0_{w_1}, 1_{w_2}\rangle \right) = \hat{a}^\dagger_{[(w_1+w_2)/\sqrt{2}]} |\tilde{0}\rangle,$$

(75)

$$|\phi_2\rangle = \frac{1}{\sqrt{2}} \left(|1_{w_1}, 0_{w_2}\rangle + i |0_{w_1}, 1_{w_2}\rangle \right) = \hat{a}^\dagger_{[(w_1+iw_2)/\sqrt{2}]} |\tilde{0}\rangle,$$

(76)

and two types of dual-rail cat qubit given by

$$|\phi_3\rangle = \frac{1}{\sqrt{2}} \left| \text{Cat}_{w_1}, \text{Squeeze}_{w_2} \right\rangle + \frac{1}{\sqrt{2}} \left| \text{Squeeze}_{w_1}, \text{Cat}_{w_2} \right\rangle$$

$$\propto \hat{a}_{[(w_1+w_2)/\sqrt{2}]} \hat{S}_r\left(\frac{w_1 + w_2}{\sqrt{2}} \right) \hat{S}_r\left(\frac{w_1 - w_2}{\sqrt{2}} \right) |\tilde{0}\rangle, \quad (77)$$

$$|\phi_4\rangle = \frac{1}{\sqrt{2}} \left| \text{Cat}_{w_1}, \text{Squeeze}_{w_2} \right\rangle - \frac{i}{\sqrt{2}} \left| \text{Squeeze}_{w_1}, \text{Cat}_{w_2} \right\rangle$$

$$\propto \hat{a}_{[(w_1-iw_2)/\sqrt{2}]} \hat{S}_r^{(2)}\left(\frac{w_1 + iw_2}{\sqrt{2}}, \frac{w_1 - iw_2}{\sqrt{2}} \right) |\tilde{0}\rangle. \quad (78)$$

Figure 4 shows the CPCA results of those four states. The left row shows the first 50 eigenvalues of C_t, that is, $\{\bar{N}_{e_j} + 1\}_{j=1}^{50}$. You can see that the first eigenvalue is outstanding in each case. Other eigenvalues, which correspond to thermal states about $|\phi_1\rangle, |\phi_2\rangle$ and squeezed states about $|\phi_3\rangle, |\phi_4\rangle$, are slightly larger than vacuum states. Due to the digital low-pass filter, those modes containing high-frequency components have small eigenvalues. It follows that the eigenvalues go below 1 as the mode index increases.

The middle row of Fig. 4 shows $e_1(t)$ plotted in real lines. The blue (dark gray) and orange (light gray) lines correspond to real and imaginary parts of $e_1(t)$. We can see that $e_1(t)$ consists of two time bins [$w_1(t)$ and $w_2(t)$]. The first time bins appear in the real part, and the second time bins appear in the real or imaginary part of $e_1(t)$. These represent the relative phases of the superposition of two time bins. As for $|\phi_1\rangle$ and $|\phi_2\rangle$, we show the theoretical predictions in the broken lines.
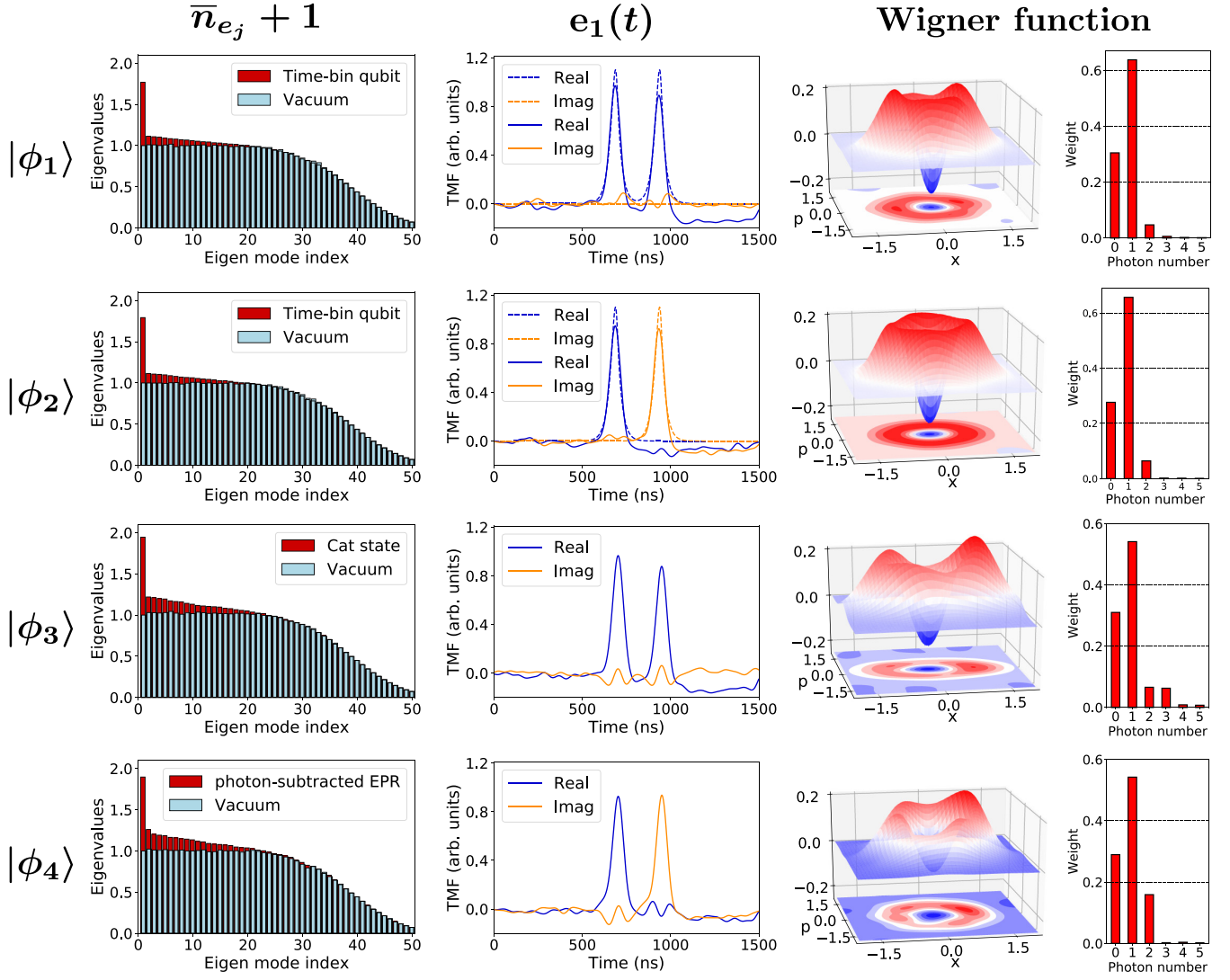
FIG. 4. Analysis results of $|\phi_1\rangle$ to $|\phi_4\rangle$. Left: First 50 eigenvalues of matrix C_t are shown in the red (dark gray) bar, and the vacuum state is shown in light blue (light gray). Middle: The first eigenfunctions $e_1(t)$ are shown in real lines. The blue (dark gray) and orange (light gray) lines show the real and imaginary parts of $e_1(t)$, respectively. As for $|\phi_1\rangle$ and $|\phi_2\rangle$, theoretical predictions are shown in the broken lines. Right: Wigner functions and photon-number distributions of e_1.

The experimental results capture the features of theoretical predictions well. Table I shows theoretically expected TMFs, the mode match of the experimental results, and the theoret-

TABLE I. Left row: analyzed states. Middle row: theoretically expected TMFs. Right row: mode match between estimated TMFs and theoretical predictions.

State	Expected TMF	Mode match
$|\phi_1\rangle$	$e_1(t) \propto w_1(t) + w_2(t)$	0.863
$|\phi_2\rangle$	$e_1(t) \propto w_1(t) + iw_2(t)$	0.912
$|\phi_3\rangle$	$e_1(t) \propto w_1(t) + w_2(t)$	0.862
$|\phi_4\rangle$	$e_1(t) \propto w_1(t) + iw_2(t)$	0.913
	$e_2(t) \propto w_1(t) - iw_2(t)$	0.630
$|\phi_5\rangle$	$f_1(t) \propto w_1(t) + iw_2(t)$	0.956
	$f_2(t) \propto w_1(t) - iw_2(t)$	0.946
$|\phi_6\rangle$	$f_1(t) \propto w_1(t) + e^{i(\pi/4)}w_2(t)$	0.827
	$f_2(t) \propto w_1(t) + e^{-i(\pi/4)}w_2(t)$	0.870

ical predictions. The mode matches are reasonably high, but some mismatch comes from mainly two reasons. One is the imperfection of the interferometer in the idler path. The mode match goes down when the power ratio or phase of the beams in the two arms of the interferometer are not set correctly. The other reason is the effect of high-pass filter after the homodyne detectors. Especially in $|\phi_1\rangle$ and $|\phi_3\rangle$, you can see that the long tail of the time bin due to the filter makes the mode match worse.

The right row of Fig. 4 shows Wigner functions and photon-number distributions of temporal mode e_1. Wigner functions have negative values, thus these states are non-Gaussian states having high nonclassicality. $|\phi_1\rangle$ and $|\phi_2\rangle$ have more than 60% single-photon components, and their Wigner functions have rotational symmetry. Thus, they are high-purity single-photon states as expected. The Wigner functions of $|\phi_3\rangle$ are squeezed in the p direction and not rotationally symmetric, which is one prominent feature of Schrödinger's cat state. From Eq. (73), $|\phi_4\rangle$ is a mixed state of
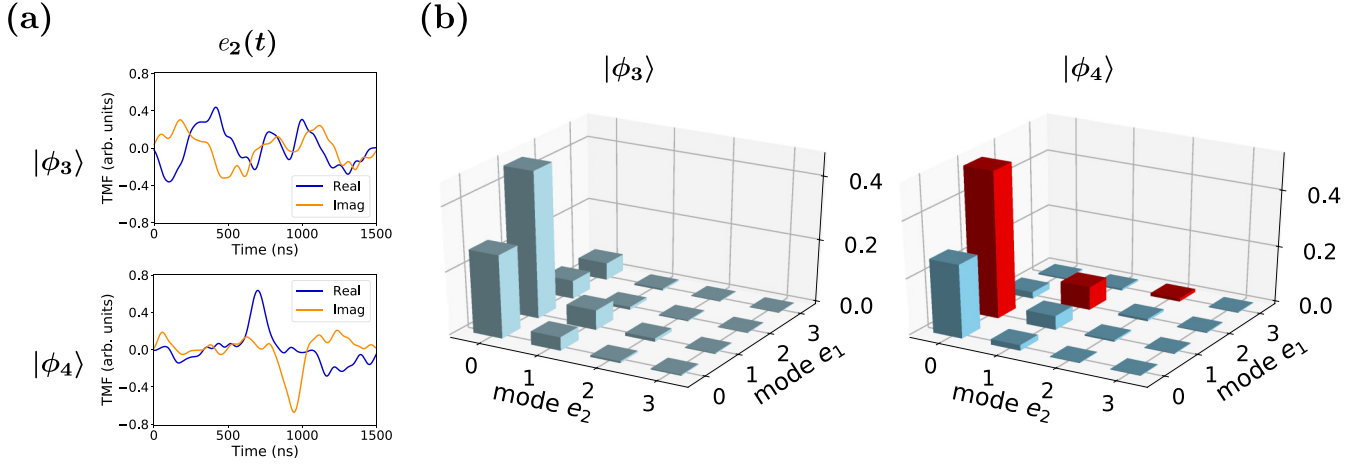
(a)

(b)

FIG. 5. (a) Second eigenfunction $e_2(t)$ of $|\phi_3\rangle$ and $|\phi_4\rangle$. (b) Two-mode photon-number distribution about e_1 and e_2. Red (dark gray) bars show expected photon-number correlation of $|\phi_4\rangle$.

$|1_{e_1}\rangle$, $|2_{e_1}\rangle$, ... in e_1, thus their Wigner function is expected to be rotationally symmetric. Actually their Wigner function is rotationally symmetric. These results confirm that the experiments have been carried out successfully.

Figure 5(a) shows $e_2(t)$ of $|\phi_3\rangle$ and $|\phi_4\rangle$. $e_2(t)$ of $|\phi_3\rangle$ has a fluctuating wave form. It is chosen to have the largest average photon number in background squeezed states. On the other hand, $e_2(t)$ of $|\phi_4\rangle$ consists of two time bins as explained in Eq. (73). In this case, however, the wave form is a little vague, and the mode match is not so high compared to other cases as shown in Table I. This may be because $\bar{N}_{e_2}$ is only slightly larger than $\bar{N}_{e_3}$, thus it becomes difficult to separate the expected mode from the background. As Eq. (73) tells, the temporal modes e_1 and e_2 of $|\phi_4\rangle$ are entangled. You can see the photon-number correlation given by $|n+1_{e_1}\rangle |n_{e_2}\rangle$ in two-mode photon-number distribution about e_1 and e_2 in Fig. 5(b). The correlation coefficient of n_{e_1} and n_{e_2} is $r = 0.498$. On the other hand, $|\phi_3\rangle$ has little photon-number correlation between e_1 and e_2 ($r = -0.015$) as shown in Fig. 5(b).

These results show that the CPCA can access the complex TMFs of various single temporal mode non-Gaussian states.

2. Results of time-bin qutrit experiments

We analyze two types of time-bin qutrits given by

$$|\phi_5\rangle = \frac{1}{\sqrt{2}} \left(|2_{w_1}, 0_{w_2}\rangle + |0_{w_1}, 2_{w_2}\rangle \right)$$
$$= \hat{a}^\dagger_{[(w_1+iw_2)/\sqrt{2}]} \hat{a}^\dagger_{[(w_1-iw_2)/\sqrt{2}]} |\tilde{0}\rangle , \qquad (79)$$

$$|\phi_6\rangle = \frac{1}{\sqrt{3}} \left(|2_{w_1}, 0_{w_2}\rangle + |1_{w_1}, 1_{w_2}\rangle + |0_{w_1}, 2_{w_2}\rangle \right)$$
$$= \hat{a}^\dagger_{\{[w_1+e^{i(\pi/4)}w_2]/\sqrt{2}\}} \hat{a}^\dagger_{\{[w_1+e^{-i(\pi/4)}w_2]/\sqrt{2}\}} |\tilde{0}\rangle . \qquad (80)$$

We can calculate $f_1(t)$ and $f_2(t)$ of these dual temporal mode two-photon states by the CPCA results in the way explained in Sec. II D. Figure 6 is the analysis result showing calculated $f_1(t)$, $f_2(t)$, Wigner functions, and photon-number distributions of those modes. The theoretical TMFs and mode match are written in Table I. Note that, in the ideal case, $|\phi_5\rangle$ satisfies $\langle f_1, f_2 \rangle = 0$ and $\bar{N}_{e_1} = \bar{N}_{e_2}$, thus we should use Eq. (64) to calculate $f_1(t)$ and $f_2(t)$. However, imperfection of experimental conditions makes $\bar{N}_{e_1} > \bar{N}_{e_2}$. Thus, we calculate $f_1(t)$, $f_2(t)$ using Eq. (63) for both $|\phi_5\rangle$ and $|\phi_6\rangle$.
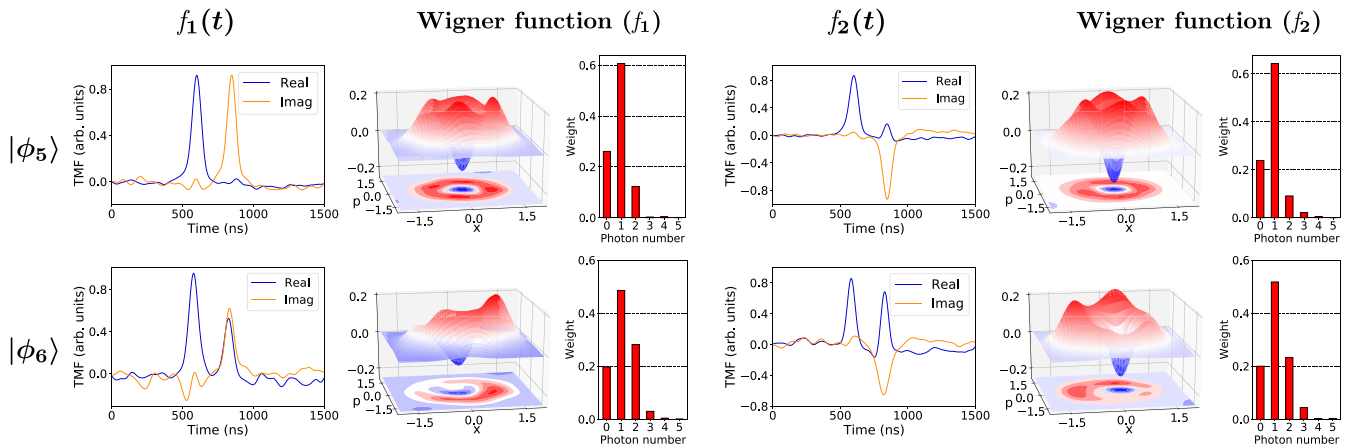

FIG. 6. Estimated $f_1(t)$, $f_2(t)$ of time-bin qutrits $|\phi_5\rangle$ and $|\phi_6\rangle$. Wigner function and photon-number distribution of each modes are also shown.

Photon-number distributions in Fig. 6 have larger weight in two-photon distribution compared to time-bin qubits in Fig. 4. One reason is that $f_1(t)$ and $f_2(t)$ are not orthogonal with inner product $|\langle f_1, f_2 \rangle| = 0.046$ for $|\phi_5\rangle$ and $|\langle f_1, f_2 \rangle| = 0.475$ for $|\phi_6\rangle$. This means that some components in mode f_1 are mixed into the mode f_2 and vice versa. This leads to larger multiphoton components in each mode. Another reason is that the two-mode squeezed vacuum contains larger multiphoton components than the time-bin qubit's case because we use higher pumping condition to have enough of a count rate of simultaneous photon detection at two APDs. Like above, we can analyze arbitrary time-bin qutrits in the way introduced in Sec. II D.

We analyzed experimentally created time-bin qubits, dual-rail cat qubits, and time-bin qutrits. These results show that the CPCA method enables us to access complex temporal mode structures of optical non-Gaussian states.

IV. CONCLUSION

We introduced the CPCA, a method to estimate complex TMFs of optical non-Gaussian states. It is based on principal components' analysis of complex variables given by continuous-wave dual-homodyne measurement. The CPCA can deal with not only arbitrary non-Gaussian states in single temporal modes, but also arbitrary two-photon states where each photon occupies a single temporal mode, which previous methods cannot deal with. We showed that our scheme works in actual situation by analyzing several experimentally non-Gaussian states. The CPCA needs only simple experimental setup, two homodyne detectors, and a continuous-wave local oscillator beam having one frequency. The analysis procedure is also simple; it is basically just a diagonalization of a matrix. Due to the simplicity and capability to characterize a wide range of quantum states, our method is a powerful tool in state creation experiments. Estimated TMFs reflect the imperfection of experiments, thus we can utilize the created states with high purity. This achievement would lead to optimization of quantum communication and quantum computation systems.

[1] E. Knill, R. Laflamme, and G. J. Milburn, Nature (London) **409**, 46 (2001).

[2] N. C. Menicucci, P. van Loock, M. Gu, C. Weedbrook, T. C. Ralph, and M. A. Nielsen, Phys. Rev. Lett. **97**, 110501 (2006).

[3] S. Takeda and A. Furusawa, Phys. Rev. Lett. **119**, 120504 (2017).

[4] S. Abruzzo, S. Bratzik, N. K. Bernardes, H. Kampermann, P. van Loock, and D. Bruß, Phys. Rev. A **87**, 052315 (2013).

[5] J. B. Brask, I. Rigas, E. S. Polzik, U. L. Andersen, and A. S. Sørensen, Phys. Rev. Lett. **105**, 160501 (2010).

[6] N. C. Menicucci, Phys. Rev. A **83**, 062314 (2011).

[7] N. C. Menicucci, Phys. Rev. Lett. **112**, 120504 (2014).

[8] J. Yoshikawa, M. Bergmann, P. van Loock, M. Fuwa, M. Okada, K. Takase, T. Toyama, K. Makino, S. Takeda, and A. Furusawa, Phys. Rev. A **97**, 053814 (2018).

[9] S. Yokoyama, R. Ukai, S. C. Armstrong, C. Sornphiphatphong, T. Kaji, S. Suzuki, J. Yoshikawa, H. Yonezawa, and A. Furusawa, Nat. Photonics **7**, 982 (2013).

[10] J. Yoshikawa, S. Yokoyama, T. Toshiyuki, C. Sornphiphatphong, Y. Shiozawa, K. Makino, and A. Furusawa, APL Photonics **1**, 060801 (2016).

[11] S. Takeda, T. Mizuta, M. Fuwa, J. Yoshikawa, H. Yonezawa, and A. Furusawa, Phys. Rev. A **87**, 043803 (2013).

[12] A. E. B. Nielsen and K. Mølmer, Phys. Rev. A **75**, 023806 (2007).

[13] C. Polycarpou, K. N. Cassemiro, G. Venturi, A. Zavatta, and M. Bellini, Phys. Rev. Lett. **109**, 053602 (2012).

[14] J. Tiedau, V. S. Shchesnovich, D. Mogilevtsev, V. Ansari, G. Harder, T. J. Bartley, N. Korolkova, and C. Silberhorn, New. J. Phys. **20**, 033003 (2018).

[15] A. MacRae, T. Brannan, R. Achal, and A. I. Lvovsky, Phys. Rev. Lett. **109**, 033601 (2012).

[16] O. Morin, C. Fabre, and J. Laurat, Phys. Rev. Lett. **111**, 213602 (2013).

[17] J. Yoshikawa, K. Makino, S. Kurata, P. van Loock, and A. Furusawa, Phys. Rev. X **3**, 041028 (2013).

[18] H. Adbi and L. J. Williams, Comput. Stat. **2**, 433 (2010).

[19] Z. Qin, A. S. Prasad, T. Brannan, A. MacRae, A. Lezama, and A. I. Lvovsky, Light: Sci. Appl. **4**, e298 (2015).

[20] I. L. Chuang, D. W. Leung, and Y. Yamamoto, Phys. Rev. A **56**, 1114 (1997).

[21] W. Wasilewaki and K. Banaszek, Phys. Rev. A **75**, 042316 (2007).

[22] M. Bergmann and P. van Loock, Phys. Rev. A **94**, 012311 (2016).

[23] M. Freyberger and W. Schleich, Phys. Rev. A **47**, R30(R) (1993).

[24] U. Leonhardt and H. Paul, Phys. Rev. A **47**, R2460(R) (1993).

[25] A. I. Lvovsky, H. Hansen, T. Aichele, O. Benson, J. Mlynek, and S. Schiller, Phys. Rev. Lett. **87**, 050402 (2001).

[26] A. I. Lvovsky and J. Mlynek, Phys. Rev. Lett. **88**, 250401 (2002).

[27] M. Yukawa, K. Miyata, T. Mizuta, H. Yonezawa, P. Marek, R. Filip, and A. Furusawa, Opt. Express **21**, 5529 (2013).

[28] M. Dakna, T. Anhut, T. Opatrný, L. Knöll, and D.-G. Welsch, Phys. Rev. A **55**, 3184 (1997).

[29] A. Ourjoumtsev, R. Tualle-Brouri, J. Laurat, and P. Grangier, Science **312**, 83 (2006).

[30] T. Gerrits, S. Glancy, T. S. Clement, B. Calkins, A. E. Lita, A. J. Miller, A. L. Migdall, S. W. Nam, R. P. Mirin, and E. Knill, Phys. Rev. A **82**, 031802(R) (2010).

[31] H. Takahashi, K. Wakui, S. Suzuki, M. Takeoka, K. Hayasaka, A. Furusawa, and M. Sasaki, Phys. Rev. Lett. **101**, 233605 (2008).

[32] D. F. Walls and G. J. Milburn, *Quantum Optics* (Springer-Verlag, Berlin, 1994).

[33] H. Takahashi, J. S. Neergaard-Nielsen, M. Takeuchi, M. Takeoka, K. Hayasaka, A. Furusawa, and M. Sasaki, Nat. Photonics **4**, 178 (2010).

[34] K. Mølmer, Phys. Rev. A **73**, 063804 (2006).